

Connecting the Unconnectable through Feedback

Yimeng Li and Yulin Shao

Abstract—Reliable uplink connectivity remains a persistent challenge for IoT devices, particularly those at the cell edge, due to their limited transmit power and single-antenna configurations. This paper introduces a novel framework aimed at connecting the unconnectable, leveraging real-time feedback from access points (APs) to enhance uplink coverage without increasing the energy consumption of IoT devices. At the core of this approach are feedback channel codes, which enable IoT devices to dynamically adapt their transmission strategies based on AP decoding feedback, thereby reducing the critical uplink SNR required for successful communication. Analytical models are developed to quantify the coverage probability and the number of connectable APs, providing a comprehensive understanding of the system’s performance. Numerical results validate the proposed method, demonstrating substantial improvements in coverage range and connectivity, particularly for devices at the cell edge, with up to a 51% boost in connectable APs. Our approach offers a robust and energy-efficient solution to overcoming uplink coverage limitations, enabling IoT networks to connect devices in challenging environments.

Index Terms—IoT, coverage analysis, feedback channel coding.

I. INTRODUCTION

In the rapidly expanding realm of the Internet of Things (IoT), reliable connectivity for devices at coverage edges remains a persistent challenge [1]–[3]. Fig. 1(a) depicts a frequently encounter situation where an IoT device at the cell edge is still able to “hear” downlink transmissions from its access point (AP), yet the AP struggles to detect the device’s uplink signals. This disparity arises from the limited transmit power and single-antenna design typical of many IoT devices, resulting in a pronounced imbalance between downlink and uplink performance. Overcoming this “unconnectable” gap is essential for unlocking the full potential of IoT applications – particularly those spanning smart cities, healthcare, and industrial automation – that demand wide and deep coverage.

To mitigate such uplink coverage limitations, conventional strategies have involved increasing uplink transmission power, employing repetitive transmissions (e.g., NB-IoT [1]), or exploiting multi-antenna diversity (e.g., the Transmission Mode (TM) 2 of LTE and TM 9 of 5G NR [2]). However, these methods are not favorable or impractical for energy-constrained, single-antenna IoT devices.

In this context, we seek an alternative that boosts uplink connectivity without raising the transmission power of IoT devices. Our proposed solution is a feedback-aided deep and wide coverage communication approach, built on the innate asymmetry between downlink and uplink communications of IoT cells. Specifically, APs typically have multiple antennas

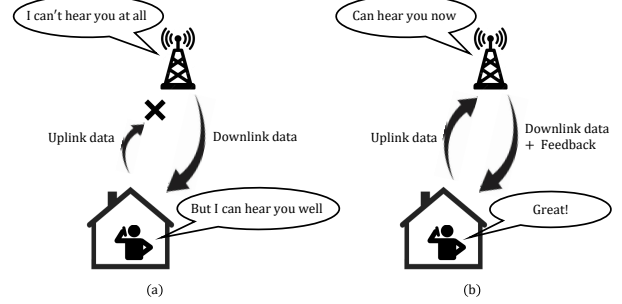


Figure 1: (a) Typical asymmetric communication scenario, where downlink is successful while uplink fails. (b) Enhanced uplink with real-time feedback, where IoT devices leverage feedback to improve uplink coverage.

and virtually unlimited power resources, allowing them to achieve extensive downlink coverage, as shown in Fig. 1(a). By exploiting this capability, the AP can transmit real-time feedback – indicating its current decoding status – to the IoT device, thereby boosting the IoT device’s uplink coding efficiency through feedback channel codes [4], [5]. As illustrated in Fig. 1(b), this feedback mechanism effectively extends the uplink coverage radius at the same device power consumption, thereby connecting the unconnectable.

The cornerstone of our proposed approach lies in the innovative use of feedback channel codes [4]–[8]. Unlike traditional forward-only error correction codes, feedback channel codes utilize real-time feedback from the AP to dynamically adjust the coding strategy and address mis-decoding at the receiver. This capability enables the receiver to decode data at much lower SNR levels, effectively extending the communication coverage. The introduction of feedback brings a dual dependency: uplink decoding performance is now influenced by both the uplink and downlink channels, a phenomenon we term dual-channel coupling. This interplay allows the AP’s abundant energy resources to be effectively utilized to extend the uplink coverage of energy-constrained IoT devices.

The contributions of this paper are summarized as follows.

- We introduce a new uplink coverage extension approach that harnesses AP’s real-time feedback to enhance the coverage probability in uplink-downlink asymmetric communications, a typical scenario in mobile edge networks.
- We quantitatively analyze the uplink coverage probabilities and the resultant number of connectable APs under the feedback-aided coverage extension paradigm. By solving the uplink-downlink dual-channel coupling, we show that real-time feedback effectively mitigates the exponential decay in coverage probability with distance, enabling the IoT device to establish links with more APs – even those previously out of reach – without increasing transmit power.

The authors are with the State Key Laboratory of Internet of Things for Smart City and the Department of Electrical and Computer Engineering, University of Macau, Macau S.A.R. (emails: {MC35385, ylishao}@um.edu.mo).

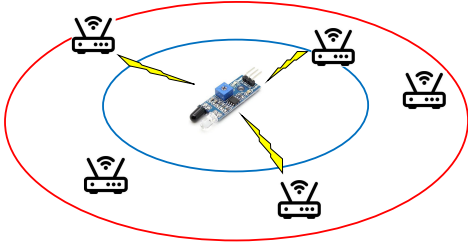


Figure 2: An IoT Device connects with distributed wireless access points. The communication can operate either in the forward mode or the feedback mode.

- Our results show that the coverage improvement is most pronounced for devices at the cell edge, where uplink SNR is weakest. By significantly boosting coverage probability in these challenging regions, the proposed feedback-based approach offers a robust pathway to “connect the unconnectable”, thereby enabling dependable IoT services in demanding environments.

II. SYSTEM MODEL

We consider an IoT environment comprising distributed wireless access points (APs). Focusing on a single IoT device, our primary interest lies in its uplink transmission coverage, specifically, the number of APs that fall within the communication range of the device with the real-time feedback from the APs.

We model the spatial distribution of the APs using a Poisson Point Process (PPP) with intensity λ , representing the average number of APs per unit area. The uplink path loss from the IoT device to an AP at a distance R can be written as

$$L_U(R) = C_U R^{-\alpha_U}, \quad (1)$$

where C_U is the uplink path loss intercepts and α_U is the uplink path loss exponents.

The transmit power of the IoT device and the AP are denoted by P_U and P_D , respectively. Due to energy constraints typical in IoT devices, we have $P_D \gg P_U$. The uplink signal-to-noise ratio (SNR) at the AP can be expressed as

$$\eta_U(R) = P_U \frac{G_t G_r L_U(R)}{\sigma_U^2} |h_U|^2, \quad (2)$$

where G_t and G_r denote the transmit and receive antenna gains, respectively; σ_U^2 is the additive white Gaussian noise (AWGN) power; h_U is the uplink small-scale fading coefficient. We model h_U by Rayleigh distribution, i.e., $|h_U|^2 \sim \text{Exp}(\mu_U)$. In this paper, we will also write SNR in decibels, in which case a ‘dB’ will be added in the subscript, e.g., $\eta_{U,\text{dB}} \triangleq 10 \lg \eta_U$.

Downlink path loss is similarly modeled but with different parameters $L_D(R) = C_D R^{-\alpha_D}$, where α_D , C_D are the respective downlink path loss exponents and intercepts. The downlink SNR received at the IoT device can be written as

$$\eta_D(R) = P_D \frac{G_t G_r L_D(R)}{\sigma_D^2} |h_D|^2, \quad (3)$$

where σ_D^2 is AWGN power; h_D is the downlink Rayleigh fading coefficient, and $|h_D|^2 \sim \text{Exp}(\mu_D)$.

To transmit a packet of K bits, the IoT device conventionally employs a forward error correction code $\mathcal{C}(K, N, \epsilon^*)$ to protect the information bits, where N is the number of uplink channel uses, and ϵ^* is the target packet error rate (PER), reflecting the target throughput. By the finite length coding theorem [9], the PER ϵ is determined by the uplink SNR η_U :

$$\sqrt{NV}Q^{-1}(\epsilon) = \frac{N}{2} \log(1 + \eta_U) - K + \mathcal{O}(\log N), \quad (4)$$

where $V = \frac{\eta_U(\eta_U+2)}{2(\eta_U+1)^2} \log^2 e$ is the channel dispersion, and Q represents the Q-function.

We refer to this conventional approach, where only forward channel coding is employed, as the forward mode. In forward mode, the critical uplink SNR required to achieve the target PER ϵ^* is denoted by Ω_c . Therefore, an AP is said to be connectable for the IoT device, or the IoT device is under the coverage of the AP, if the uplink SNR $\eta_U \geq \Omega_c$.

When the AP provides real-time feedback to the IoT device, the channel coding efficiency can be significantly improved. This enhancement effectively lowers the critical uplink SNR required to achieve the target PER, thereby increasing the probability that an AP at any distance R is connectable. We refer to this enhanced communication approach as the feedback mode.

In feedback mode, the IoT device employs a feedback error correction code $\mathcal{C}_f(K, N, N', \epsilon^*)$, where K , N , ϵ^* are as defined in $\mathcal{C}(K, N, \epsilon^*)$, while N' is the number of downlink channel uses dedicated to feedback. In this paper, we consider the feedback coding architecture in [6], [8], in which case $N' = aN$, where $a \in \mathbb{Z}^+$ is a positive integer. The critical uplink SNR in the feedback mode required to meet the target ϵ^* , denoted as Ω_f , follows a logistic function:

$$\Omega_{f,\text{dB}} = \frac{1}{\exp(u_0 \eta_{D,\text{dB}} + u_1 a + u_2 \eta_{D,\text{dB}} a + u_3) + u_4} + u_5, \quad (5)$$

where $\{u_0, u_1, u_2, u_3, u_4, u_5\}$ are constants, determined by the target PER ϵ^* . An AP is deemed connectable for the IoT device if the uplink SNR $\eta_U \geq \Omega_f$.

As can be seen from (5), unlike the critical SNR Ω_c in the forward mode, which depends solely on the target PER ϵ^* , the critical SNR Ω_f in the feedback mode also depends on the feedback channel quality η_D and allocated feedback channel resources a . Consequently, Ω_f becomes a random variable due to the inherent randomness of the downlink channel quality η_D . This dual dependency – on both uplink and downlink channel conditions – introduces a unique coupling effect between the two channels. Specifically, the uplink channel determines the IoT device’s ability to meet the SNR threshold for a given distance to the AP, while the downlink channel impacts the efficiency of feedback communication, which in turn affects the required critical SNR in the uplink.

III. UPLINK COVERAGE ANALYSIS WITH FEEDBACK

In this section, we analyze the number of APs that are connectable in the feedback mode and quantify the performance

gains achieved by leveraging real-time feedback. Specifically, we focus on a circular coverage area centered around the IoT device with radius D . The number of connectable APs in this feedback scenario is denoted as $M_f(D)$.

In feedback mode, the interplay between the uplink and downlink channels introduces a coupled dual-channel fading behavior. This coupling complicates the analysis of feedback communication systems, as the statistical properties of both the uplink and downlink channels must be jointly considered. Accurately characterizing this interdependence is critical for evaluating the system's coverage performance.

We define the probability that an AP at a distance R is connectable under feedback mode as $\varphi_f(R) \triangleq \Pr(\eta_U(R) \geq \Omega_f)$. Note that both $\eta_U(R)$ and Ω_f are random variables: the randomness of $\eta_U(R)$ arises due to uplink small-scale fading, while the randomness of Ω_f is introduced through the downlink SNR $\eta_D(R)$, which influences the feedback quality.

Substituting the expression for $\eta_U(R)$ into $\varphi_f(R)$, the coverage probability can be reformulated as

$$\varphi_f(R) = \Pr\left(|h_U|^2 > \frac{\Omega_f \sigma_U^2}{P_U G_t G_r C_U R^{-\alpha_U}}\right). \quad (6)$$

To simplify the notation, we introduce a function $g(R, |h_D|^2)$:

$$g(R, |h_D|^2) \triangleq \frac{\Omega_f \sigma_U^2}{P_U G_t G_r C_U R^{-\alpha_U}},$$

where Ω_f , as given in (5), is governed by the downlink received SNR η_D .

Since both $|h_U|^2$ and $|h_D|^2$ follow exponential distributions, the coverage probability can be rewritten as

$$\begin{aligned} \varphi_f(R) &= \Pr\left(|h_U|^2 > g(R, |h_D|^2)\right) \\ &= \int_0^{+\infty} [1 - (1 - e^{-\mu_U g(R, |h_D|^2)})] f(|h_D|^2) d|h_D|^2 \\ &= \int_0^{+\infty} e^{-\mu_U g(R, x)} \mu_D e^{-\mu_D x} dx \\ &\stackrel{(a)}{\approx} \sum_{k=1}^K w_k e^{-\mu_U g\left(R, \frac{x_k}{\mu_D}\right)}, \end{aligned} \quad (7)$$

where $f(x)$ is the probability density function (PDF) of the exponential distribution; (a) follows from the Gauss-Laguerre quadrature [10], in which x_k represents the roots of the Laguerre polynomials and w_k are the weights associated with these roots.

To derive the number of connectable APs, an accurate approximation of $g(R, |h_D|^2)$ is necessary. We start by approximating the downlink SNR in decibels, denoted as $\eta_{D,dB}\left(\frac{x_k}{\mu_D}\right)$, as follows:

$$\begin{aligned} \eta_{D,dB}\left(\frac{x_k}{\mu_D}\right) &= 10 \lg\left(\frac{P_D G_t G_r C_D x_k R^{-\alpha_D}}{\mu_D \sigma_D^2}\right) \\ &= 10 \lg(Z_{1,k} R^{-\alpha_D}) = 10 \lg Z_{1,k} + 10 \lg R^{-\alpha_D} \\ &= 10 \lg Z_{1,k} + \frac{10}{\ln 10} \ln R^{-\alpha_D} \\ &\approx 10 \lg Z_{1,k} + \frac{10}{\ln 10} (R^{-\alpha_D} - 1), \end{aligned} \quad (8)$$

where $Z_{1,k} \triangleq \frac{P_D G_t G_r C_D x_k}{\mu_D \sigma_D^2}$ and $Z_2 \triangleq \frac{\sigma_U^2}{P_U G_t G_r C_U}$ encapsulates system parameters for the downlink and uplink, respectively.

Substituting (8) into (5), the critical SNR in decibels $\Omega_{f,dB}$ can be approximated as

$$\Omega_{f,dB} \approx \frac{1}{\exp(B_{1,k} + B_2 R^{-\alpha_D} - 1 - u_4) + u_4} + u_5, \quad (9)$$

where $B_{1,k} = 1 + u_1 a + u_3 + u_4 + 10(u_0 + u_2 a)(\lg Z_{1,k} - \frac{1}{\ln 10})$ and $B_2 = \frac{10}{\ln 10}(u_0 + u_2 a)$.

Using the first-order Taylor series expansion $e^x = 1 + x + R_1^{(1)}$, the approximation of $\Omega_{f,dB}$ becomes

$$\Omega_{f,dB} \approx \frac{1}{B_{1,k} + B_2 R^{-\alpha_D} + R_1^{(1)}} + u_5. \quad (10)$$

Applying another Taylor series expansion $\frac{1}{1+x} = 1 - x + R_1^{(2)}$, we further simplify $\Omega_{f,dB}$ as

$$\Omega_{f,dB} \approx \frac{1}{B_{1,k}} \left(1 - \frac{B_2}{B_{1,k}} R^{-\alpha_D} - \frac{R_1^{(1)}}{B_{1,k}} + R_1^{(2)} + u_5 B_{1,k}\right). \quad (11)$$

Here, the bounds of the Lagrange remainder terms satisfy $R_1^{(1)} \geq 0$ and $R_1^{(2)} \geq 0$.

We now approximate $g\left(R, \frac{x_k}{\mu_D}\right)$, defined as the effective threshold function:

$$\begin{aligned} g\left(R, \frac{x_k}{\mu_D}\right) &= Z_2 R^{\alpha_U} 10^{\frac{1}{10} \Omega_{f,dB}} \\ &= Z_2 R^{\alpha_U} e^{\frac{\ln 10}{10} \Omega_{f,dB}} = Z_2 R^{\alpha_U} \left(1 + \frac{\ln 10}{10} \Omega_{f,dB} + R_1^{(3)}\right), \end{aligned} \quad (12)$$

where $R_1^{(3)}$ represents the remainder of the Taylor expansion.

Substituting (11) into (12), we obtain

$$\begin{aligned} g\left(R, \frac{x_k}{\mu_D}\right) &\approx Z_2 R^{\alpha_U} \left[1 + \frac{\ln 10}{10 B_{1,k}} \left(1 - \frac{B_2}{B_{1,k}} R^{-\alpha_D} \right. \right. \\ &\quad \left. \left. - \frac{R_1^{(1)}}{B_{1,k}} + R_1^{(2)} + u_5 B_{1,k}\right) + R_1^{(3)}\right]. \end{aligned} \quad (13)$$

In particular, the Lagrange form of the remainder $R_1^{(3)}$ can be approximated by

$$\begin{aligned} R_1^{(3)} &= \frac{1}{2!} e^{\frac{\ln 10}{10 B_{1,k}} \left(1 - \frac{B_2}{B_{1,k}} R^{-\alpha_D} - \frac{R_1^{(1)}}{B_{1,k}} + R_1^{(2)} + u_5 B_{1,k}\right)} \\ &\quad \times \left[\frac{\ln 10}{10 B_{1,k}} \left(1 - \frac{B_2}{B_{1,k}} R^{-\alpha_D} - \frac{R_1^{(1)}}{B_{1,k}} + R_1^{(2)} + u_5 B_{1,k}\right) \right]^2 \\ &\approx \frac{1}{2} \left[\frac{\ln 10}{10 B_{1,k}} \left(1 - \frac{B_2}{B_{1,k}} R^{-\alpha_D} - \frac{R_1^{(1)}}{B_{1,k}} + R_1^{(2)} + u_5 B_{1,k}\right) \right]^2. \end{aligned} \quad (14)$$

Since $R_1^{(1)} \geq 0$, $R_1^{(2)} \geq 0$, and $(1+x)^\alpha \approx 1 + \alpha x$, $R_1^{(3)}$ can be further refined as

$$\begin{aligned} R_1^{(3)} &\approx \frac{\ln^2 10}{200 B_{1,k}^2} (1 + u_5 B_{1,k})^2 \left[1 - \frac{B_2 R^{-\alpha_D}}{B_{1,k}(1 + u_5 B_{1,k})}\right]^2 \\ &\approx \frac{\ln^2 10}{200 B_{1,k}^2} (1 + u_5 B_{1,k})^2 \left[1 - \frac{2 B_2 R^{-\alpha_D}}{B_{1,k}(1 + u_5 B_{1,k})}\right]. \end{aligned} \quad (15)$$

Substituting (15) into (13) yields

$$g\left(R, \frac{x_k}{\mu_D}\right) \approx J_{1,k} R^{\alpha_U} - J_{2,k}, \quad (16)$$

where $J_{1,k} \triangleq Z_2 + \frac{Z_2(1+u_5 B_{1,k}) \ln 10}{10 B_{1,k}} + \frac{Z_2(1+u_5 B_{1,k})^2 \ln^2 10}{200 B_{1,k}^2}$ and $J_{2,k} \triangleq \frac{Z_2 B_2 \ln 10}{10 B_{1,k}^2} + \frac{Z_2 B_2(1+u_5 B_{1,k}) \ln^2 10}{100 B_{1,k}^3}$.

Given the coverage probability $\varphi_f(R)$, the number of connectable APs $M_f(D)$ within a circular area of radius D can be expressed as

$$\begin{aligned} M_f(D) &= \int_0^D \varphi_f(R) \lambda 2\pi R dR \\ &\approx \int_0^D \sum_{k=1}^K w_k e^{-\mu_1 g\left(R, \frac{x_k}{\mu_D}\right)} \lambda 2\pi R dR \\ &= 2\pi\lambda \sum_{k=1}^K w_k \int_0^D e^{-\mu_1 g\left(R, \frac{x_k}{\mu_D}\right)} R dR, \end{aligned} \quad (17)$$

Substituting the approximation of $g\left(R, \frac{x_k}{\mu_D}\right)$ in (16), we finally have

$$\begin{aligned} M_f(D) &\approx 2\pi\lambda \sum_{k=1}^K w_k e^{\mu_U J_{2,k}} \int_0^D e^{-\mu_U J_{1,k} R^{\alpha_U}} R dR \\ &= 2\pi\lambda \sum_{k=1}^K w_k e^{\mu_U J_{2,k}} \frac{\gamma\left(\frac{2}{\alpha_U}, \mu_U J_{1,k} D^{\alpha_U}\right)}{(\mu_U J_{1,k})^{\frac{2}{\alpha_U}} \alpha_U}. \end{aligned} \quad (18)$$

where $\gamma(\cdot, \cdot)$ is lower incomplete gamma function.

To provide a benchmark for comparison with the feedback mode, we derive the number of connectable APs in the forward mode, where no feedback is employed, and the coverage performance depends solely on the uplink channel conditions. Let $M_c(D)$ denote the number of connectable APs within a circular area of radius D . This can be similarly expressed as $M_c(D) = \int_0^D \varphi_c(R) \lambda 2\pi R dR$, where $\varphi_c(R)$ represents the probability that a AP at a distance R is connectable in forward mode. Specifically, we have

$$\varphi_c(R) = \Pr(\eta_U(R) \geq \Omega_c) = e^{-AR^{\alpha_U}}, \quad (19)$$

where $A \triangleq \frac{\mu_U \Omega_c \sigma_V^2}{P_U G_t G_r C_U}$. Substituting (19) into $M_c(D)$, the number of connectable APs in forward mode is given by

$$M_c(D) = 2\pi\lambda \int_0^D e^{-AR^{\alpha_U}} R dR = \frac{2\pi\lambda \cdot \gamma\left(\frac{2}{\alpha_U}, AD^{\alpha_U}\right)}{\alpha_U A^{\frac{2}{\alpha_U}}}. \quad (20)$$

Remark (Coverage probability improvement with feedback). *The comparison between the coverage probabilities $\varphi_c(R)$ in forward mode and $\varphi_f(R)$ in feedback mode highlights the substantial improvement brought by feedback.*

In forward mode, the coverage probability decays exponentially with distance R , as captured by the fixed term $e^{-AR^{\alpha_U}}$, which depends solely on the uplink channel quality. In contrast, feedback mode leverages both uplink and downlink channels, where the feedback gains are encapsulated in the terms $J_{1,k}$ and $J_{2,k}$. These terms effectively reduce the required critical SNR, thereby slowing down the decay in coverage probability as R increases.

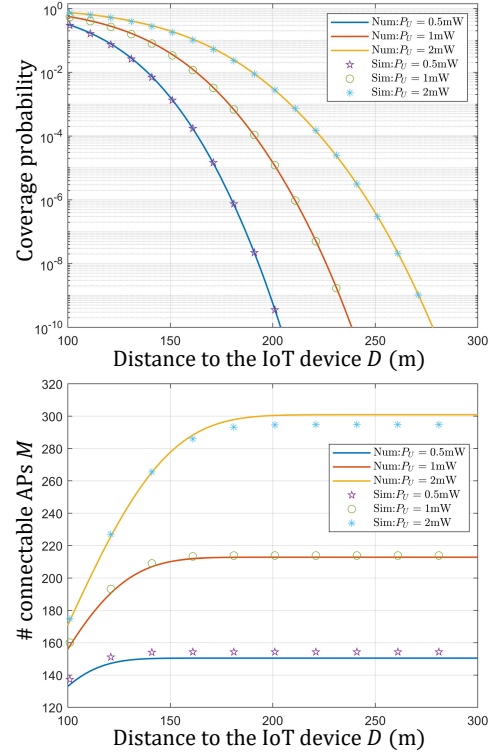


Figure 3: Comparison of analytical and simulation results for validating the accuracy of the analytical expressions, where $P_U \in [0.5, 1, 2]$ mW, $P_D = 50$ mW, $a = 1$, and $\lambda = 6 \times 10^{-3}$.

This improvement is particularly pronounced at larger distances, such as at the cell edge, where the uplink SNR is typically weak, and connectivity is more prone to failure. By increasing the coverage probability through feedback, the connectivity in these edge regions can be significantly enhanced.

IV. NUMERICAL RESULTS

This section evaluates the performance of the proposed feedback-aided coverage enhancement approach through numerical simulations. To establish an evaluation framework, we configure the system parameters as follows. The density of APs is set to $\lambda = 6 \times 10^{-3}$, with path loss exponents and intercepts set as $C_U = C_D = 10^{-4.7}$ and $\alpha_U = \alpha_D = 4$ [11]. The uplink and downlink Rayleigh fading channels are modeled with parameters $\mu_U = \mu_D = 2$. We consider a short block length $K = 48$, a code rate of $1/3$, resulting in $N = 144$ channel uses, and a target uplink PER $\epsilon^* = 10^{-4}$. In the forward mode, Polar and Turbo codes with the same block length and coding rate are utilized as benchmarks, enabling a direct comparison of their performance against the proposed feedback-aided approach. The downlink transmit power is fixed at $P_D = 50$ mW, while the uplink transmit power is varied across $P_U \in [0.5, 1, 2]$ mW to examine the impact of different power levels on system performance.

We begin by verifying the accuracy of the analytical models established for feedback-aided connectivity in Section III. To this end, we compare the derived expressions for the number of connectable APs with simulation results, as illustrated

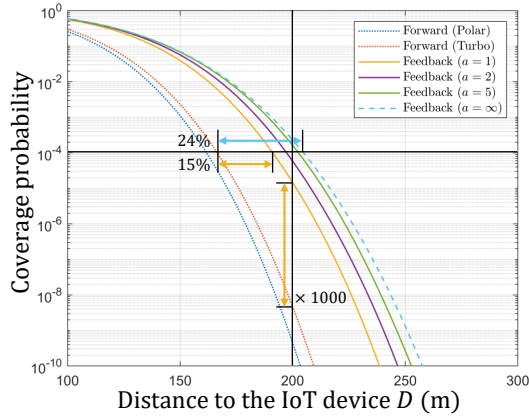


Figure 4: The coverage probability gains of the feedback mode versus the forward mode with Polar and Turbo codes.

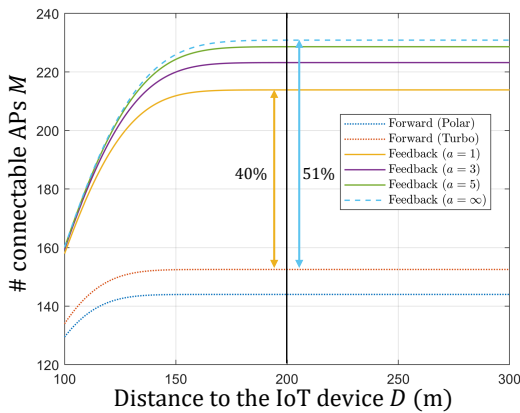


Figure 5: The gains in the number of connectable APs achieved by the feedback mode versus the forward mode using Polar and Turbo codes.

in Fig. 3. This comparison focuses on two key steps: the approximations of coverage probability and the computation of connectable APs. The results in Fig. 3 reveal a strong alignment between the analytical predictions and simulation outcomes across varying uplink transmit power levels and distances to the IoT device. This close match confirms the validity and robustness of our analytical method, demonstrating its effectiveness as a reliable tool for evaluating feedback-aided IoT coverage performance.

Next, we explore the transformative impact of feedback on connecting previously unreachable APs. Fig. 4 illustrates the substantial enhancement in coverage probability achieved through feedback at varying distances. Notably, its benefits are most pronounced at larger distances, particularly for IoT devices situated at the cell edge. At 200 meters, for instance, feedback boosts the coverage probability by three orders of magnitude, effectively bridging the gap where traditional forward-only communication fails. The extent of this improvement is closely tied to the amount of feedback, a . More feedback allows the user to precisely assess the decoding status of the AP, significantly extending the coverage range. Without feedback, Turbo codes ensure a coverage probability of 10^{-4} up to 166 meters. In stark contrast, feedback extends

this reliability to 205 meters – a remarkable 24% increase in range, enabling connections far beyond the traditional limits.

The benefits of feedback extend beyond probability gains. Fig. 5 showcases the number of connectable APs, M , at varying distances. At a distance of 200 meters, feedback enhances the number of reachable APs by 51%, transforming what was previously an unconnected region into a significantly more connected zone. These results emphasize the power of feedback in “connecting the unconnectable”, redefining the boundaries of IoT network performance.

V. CONCLUSIONS

This work has laid the groundwork for a transformative approach to enhancing IoT uplink connectivity through feedback-aided communication. By introducing and analyzing the dual-channel coupling effect, we have shown that real-time feedback fundamentally redefines the coverage possibilities in edge scenarios. Our findings underscore the strategic use of feedback to counteract the asymmetry between uplink and downlink performance, bridging what was previously an “unconnectable” gap.

Beyond validating the proposed approach, this paper represents a paradigm shift in IoT network design. The results highlight the potential of feedback-based systems to maximize connectivity and energy efficiency, providing a robust foundation for practical deployment in real-world systems. Future work would explore the scalability of this framework in diverse network topologies and dynamic environments. Additionally, integrating advanced techniques, such as multi-device coordination or adaptive signal processing, could further extend the capabilities of IoT networks, steering them toward more intelligent, adaptable, and sustainable solutions.

REFERENCES

- [1] M. Kanj, V. Savaux, and M. Le Guen, “A tutorial on NB-IoT physical layer design,” *IEEE Communications Surveys & Tutorials*, vol. 22, no. 4, pp. 2408–2446, 2020.
- [2] S. Parkvall, E. Dahlman, A. Furuskar, and M. Frenne, “NR: The new 5G radio access technology,” *IEEE Communications Standards Magazine*, vol. 1, no. 4, pp. 24–30, 2017.
- [3] Y. Shao, D. Gündüz, and S. C. Liew, “Federated edge learning with misaligned over-the-air computation,” *IEEE Transactions on Wireless Communications*, vol. 21, no. 6, pp. 3951–3964, 2021.
- [4] C. Shannon, “The zero error capacity of a noisy channel,” *IRE Trans. Inf. Theory*, vol. 2, no. 3, pp. 8–19, 1956.
- [5] Y. Polyanskiy, H. V. Poor, and S. Verdú, “Feedback in the non-asymptotic regime,” *IEEE Transactions on Information Theory*, vol. 57, no. 8, pp. 4903–4925, 2011.
- [6] Y. Shao, “DEEP-IoT: Downlink-enhanced efficient-power Internet of Things,” *IEEE Transactions on Wireless Communications*, 2024.
- [7] J. Schalkwijk and T. Kailath, “A coding scheme for additive noise channels with feedback I: No bandwidth constraint,” *IEEE Trans. Inf. Theory*, vol. 12, no. 2, pp. 172–182, 1966.
- [8] E. Ozfatura, Y. Shao, A. G. Perotti, B. M. Popović, and D. Gündüz, “All you need is feedback: Communication with block attention feedback codes,” *IEEE Journal on Selected Areas in Information Theory*, vol. 3, no. 3, pp. 587–602, 2022.
- [9] Y. Polyanskiy, H. V. Poor, and S. Verdú, “Channel coding rate in the finite blocklength regime,” *IEEE Transactions on Information Theory*, vol. 56, no. 5, pp. 2307–2359, 2010.
- [10] N. I. Ioakimidis, “The Gauss-Laguerre quadrature rule for finite-part integrals,” *Communications in numerical methods in engineering*, vol. 9, no. 5, pp. 439–450, 1993.
- [11] T. Bai and R. W. Heath, “Coverage and rate analysis for millimeter-wave cellular networks,” *IEEE Transactions on Wireless Communications*, vol. 14, no. 2, pp. 1100–1114, 2015.